Desalination and Water Treatment
www.deswater.com

doi: 10.5004/dwt.2020.24941

178 (2020) 110–122
February

Denitrification performance and kinetics of an attapulgite lightweight ceramsite biofilter

ZiJie Wang, Zheng Wang*, Kai Xu, Lei Chen, ZiZeng Lin, YaLi Liu

School of Civil Engineering, Nanjing Forestry University, Longpan Road 159#, Nanjing 210037, China, Tel. +86 25 85427691; emails: wangzheng@njfu.edu.cn (Z. Wang), wzj854333843@163.com (Z.J. Wang), horizonxk@163.com (K. Xu), clymcl@163.com (L. Chen), ccitlin@163.com (Z.Z. Lin), liuyali0418@163.com (Y.L. Liu)

Received 26 April 2019; Accepted 22 September 2019

ABSTRACT

Operating costs and nitrogen removal performance are the most critical aspects of biological nitrogen removal technologies. Here, an attapulgite clay lightweight ceramsite (ACLC) was successfully prepared and combined with a denitrifying biofilter (DNBF) to cost-effectively treat nitrogen-contaminated water. Scanning electron microscopy and Fourier transform infrared spectroscopy were used to characterize the ACLC. Bacteria adhered easily to the ACLC, and biofilm formation was rapid. ACLC density was close to that of water; ACLC floated on the water surface. The optimal parameters of the DNBF were as follows: a hydraulic load of 2.0 $m^3/(m^2\ h)$, a carbon to nitrogen ratio of 4:1, and an anhydrous sodium acetate carbon source. With these optimal parameters, the efficiency of removal of total nitrogen and NO_3^--N were 87% and 90%, respectively, and the accumulation of NO_2^-–N concentration was 0.18 mg/L. The recovery speed of the DNBF after backwashing, as well as after 3 and 6 d outages, was rapid: only 6 h. The biological denitrification kinetics of the DNBF indicated that a first-order reaction more accurately described the DNBF denitrification process, with a correlation coefficient (R^2) of 0.993.

Keywords: Nitrogen removal; Attapulgite clay; Lightweight ceramsite; Denitrifying biofilter; Biological denitrification kinetics

1. Introduction

Nitrogen pollution may cause the excessive growth of aquatic plants and algae, leading to eutrophication and water-quality deterioration [1,2]. Toxic algae blooms and reduced biodiversity can also be caused by excessive nitrogen in the aquatic environment [3]. The data from the Global Environmental Monitoring System shows that the nitrate concentrations are seven times as high as the allowable maximum pollutant concentration (45 mg/L) in most rivers [4]. In the EU and North America, wastewaters discharged into sensitive water bodies are required to have total nitrogen (TN) concentrations <3 mg/L [5]. Therefore, it is very important to remove nitrogen from wastewater to reduce ecological risks.

Despite the shortcomings of high sludge yield, biological nitrogen removal is still one of the most effective ways to eliminate nitrogen pollution in water [1,6,7]. The denitrification reaction primarily relies on heterotrophic microorganisms that use NO_3^- and NO_2^- as electron acceptors. During this process, NO_3^- is first reduced to NO_2^-, and then NO_2^- is reduced to a gaseous compound [8]. As denitrifying biofilters (DNBFs) are highly efficient, require little floor space, and have a small impact load, these are widely used to remove nitrogen pollution [9]. Moreover, since DNBFs combine physical filtration and biological treatment, sludge expansion is not a concern. The core of the DNBF is the biofilm, which is adsorbed on the filter material. Biofilms form and grow in three stages: attachment, maturation, and aging.

* Corresponding author.

Between these stages, the structure of the biofilm changes, which may lead to changes in the nitrate/nitrite reduction rate and enzyme activity [10]. Thus, the biofilm structure affects both DNBF denitrification performance and nitrite accumulation [11].

The filter material used in the DNBF is critical, as this substance acts as the biofilm carrier [12]. The most commonly used filter materials are quartz sand, ceramsite, zeolite, etc [13]. However, these filter materials are usually prepared in a heavy form. Heavy filter materials have large specific gravities, and the use of such materials as biofilm carriers leads to high backwash energy consumption, large head loss, and high operating costs [14]. Therefore, recent studies have focused on the development of lightweight filter materials [15]. Lightweight filter materials are of low quality, reducing the mechanical energy required for filter operation and backwashing, and thus resulting in significant reductions in energy demands and operation costs [16].

Clay minerals have recently received much research attention due to their high surface area, layered structure, low cost, non-toxicity, accessibility, and chemical stability [17,18]. Numerous studies have used clay minerals to remove contaminants, particularly heavy metal ions, and other organics, from aqueous solutions [19,20]. Attapulgite clay, which is primarily composed of attapulgite, is an aqueous, magnesium-rich aluminosilicate clay mineral with a chain structure [21]. Attapulgite clay is a natural resource that has good environmental compatibility and has high capacities for both adsorption and absorption. This clay is widely used in wastewater treatment, sensing, painting, and other fields [22]. Previous studies have indicated that attapulgite clay effectively removes organic matter and heavy metals [23]. However, the combination of attapulgite clay and lightweight filter material has not been applied to the study of DNBF. Therefore, in this study, we established a method for preparing attapulgite clay lightweight ceramsite (ACLC) biofilter and applied ACLC to a DNBF to remove nitrogen pollution.

The objectives of this study were as follows: (1) to evaluate the surface properties of ACLC after preparation, (2) to study the factors influencing the ACLC DNBF, (3) to fit the experimental data to a kinetic denitrification model, and (4) to analyze the denitrification mechanisms of the ACLC DNBF.

2. Materials and methods

2.1. Materials and analysis methods

The primary chemicals used in this study were pure and of analytical grade; the experimental water was deionized. All chemicals used in this experiment were purchased from Nanjing Chemical Reagent Co. Ltd., China. The raw materials related to the preparation of the ACLC were provided by Anhui Huasheng Environmental Protection Technology Co. Ltd., China. Activated sludge was provided by the Nanjing Chengbei Wastewater Treatment Plant, China. The tested parameters and methods are shown in Table 1.

The "raw water" used in this experiment was artificially constructed and primarily consisted of glucose, sodium nitrate, ammonium chloride, and a small amount of potassium dihydrogen phosphate. In the raw water, the TN concentration was ~20 mg/L, and the nitrate concentration was ~8 mg/L.

Table 1
Test items and methods

Parameter	Method
TN	Potassium persulfate oxidation-ultraviolet spectrophotometry
NO_2^-–N	N-(1-Naphthalene)-Ethylenediamine dihydrocholride spectrophotometry
NO_3^-–N	Phenol disulfonic acid spectrophotometry
DO	Multi-parameter water quality tester (MP3500; Alalis, China)
pH	pH meter (pH400; Alalis, China)

2.2. Preparation of ACLC

The ACLC preparation method included the following steps: mixing, granulating, drying, calcining, secondary granulating, secondary drying, and secondary calcining. First, sieved and dried toner, feldspar, bentonite, fluorite powder, and deionized water were mixed in appropriate proportions. Sodium sulfate and magnesium carbonate were then added to form a slurry. Second, the slurry was pelleted in a granulator (QJ-500; Purui, China), and the pellets were dried in an oven (GZX-9140MBE; Boxun, China) at 105°C for 120 min to remove moisture. Third, the dried pellets were quickly transferred to a muffle furnace (SX-12–10; Tester, China). The temperature in the muffle furnace was increased at a rate of 15°C/min to 800°C and then held at 800°C for 120 min. Fourth, the material was removed from the furnace and cooled to ambient temperature to obtain the semi-finished product. Fifth, the semi-finished product and the attapulgite clay were mixed in appropriate proportions. Then, this mixture was placed in the granulator for secondary granulation. Sodium silicate adhesive was sprayed on the material during ball formation. Sixth, after drying at 105°C for 120 min in the oven, the material was placed in a muffle furnace. The temperature in the muffle furnace was increased at a rate of 15°C/min to 800°C and then held at 800°C for 120 min. Finally, the material was then removed from the furnace and cooled to ambient temperature; this material was the ACLC (Fig. 1).

2.3. Characteristic methods

The Brunauer-Emmett-Teller (BET) surface area of the ACLC was measured using a fully automatic specific-surface area and pore-size distribution meter (Autosorb iQ; Conta, USA). The dry and wet bulk densities of the ACLC were measured with a bulk density tester (ST-102; Lugong, China). The ACLC particle size distribution was measured with a laser particle size analyzer (Winner 2000; Jinan Micron, China). High-resolution ACLC images were captured using an environmental scanning electron microscopy (SEM) (Quanta 200; FEI, USA). As the ACLC is a poor conductor, we crushed and dried the ACLC, affixed it to a

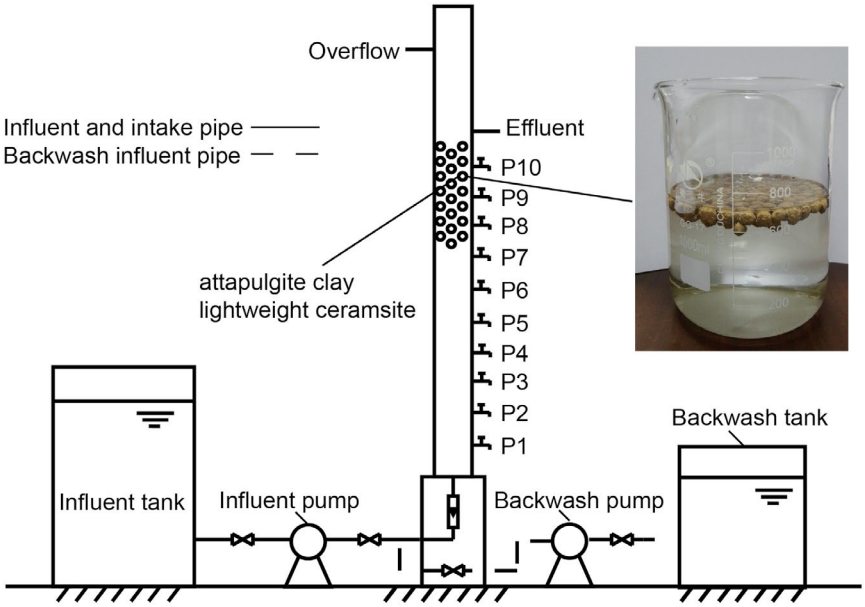

Fig. 1. Experimental schematic of DNBF with ACLC.

copper mesh, and vaporized the conductive layer for measurement. The accelerating voltage was 20 kV, and the ACLC image prior to use was taken at 2,000× and 4,000× magnification. The ACLC image after use was taken at 5,000× and 8,000× magnification. The functional groups of the ACLC were identified using Fourier-transform infrared spectroscopy (FT-IR) (Nicolet IS5; Thermo Scientific, USA). A small volume of ACLC was dried, ground into a powder, and mixed with a 300 times volume of potassium bromide to prepare a potassium bromide tablet. The scanning waves were 10–15,500 cm^{-1}, with a resolution of 0.2 cm^{-1}.

2.4. Details of the DNBF system

The DNBF (Fig. 1) was a cylindrical Plexiglas column, with a height of 3 m and a bottom area of approximately 0.785 dm^2. The internal structure of the filter column (from bottom to top) comprised a support zone, a packing zone, and a clear water area [24]. The sampling ports (P1–P10) were set every 20 cm above the support zone. The packing zone was filled with ACLC. Influent and backwash water pipes were located at the bottom of the filter column; influent was pumped in. The reactor was an up-flow reactor, and effluent was discharged from the top overflow. The additional carbon source was pumped into the filter column from the bottom with a peristaltic pump.

2.5. Experimental methods

The experiment was conducted in two phases: the start-up phase (30 d) and the single factor experimental phase (38 d). The start-up phase, which was divided into two steps, was the continuous cultivation of membranes. First, the domestic sewage from Nanjing Forestry University (China) was mixed with the raw water at a ratio of 1:10. The total volume of the mixed solution was 500 L. The activated sludge from Nanjing Chengbei Wastewater Treatment Plant (China) was added to the mixed solution, and this combined solution was run for 2 d. After this point, the film was hung on the reactor. The hydraulic load of the membrane was 3.14 $m^3/(m^2\ h)$, and the carbon source (with sodium acetate added) had a carbon to nitrogen ratio of 3.5:1.

During the single factor experimental phase, we analyzed the effects of different carbon source types, dosages, hydraulic loads, and backwashing conditions on the denitrification efficiency of the DNBF reactor. We also tested the recovery of the denitrification efficiency of the DNBF reactor after intermittent operation. This five-phase experiment was designed to identify the best-operating conditions for the ACLC DNBF.

First, we examined the effects of hydraulic load on the denitrification performance of the DNBF. In this phase, the denitrification biofilter operated stably for 6 h, the carbon source was anhydrous sodium acetate, and the carbon to nitrogen ratio of 3.5:1. We measured denitrification efficiency, pH, and dissolved oxygen (DO) using 20, 40, 60, 80, and 100 cm filter columns, at hydraulic loads of 1.4, 2.0, 3.0, 4.0, 5.0, 6.0, and 7.0 $m^3/(m^2\ h)$. Each hydraulic load experiment was repeated twice, and the results were averaged.

Second, we examined how changes in the carbon to nitrogen ratio affected the denitrification performance of the DNBF. In this test, the denitrification biofilter operated stably; the influent and the carbon source were anhydrous sodium acetate, and hydraulic load was 2.0 $m^3/(m^2\ h)$. The carbon to nitrogen ratios we tested were 3:1, 3.5:1, 4:1, and 4.5:1. Based on the DNBF effluent, we identified the optimal carbon to nitrogen ratio. Each carbon-nitrogen experiment was repeated three times, and the results were averaged.

Third, we investigated the effects of different carbon sources on DNBF denitrification performance. In this

experiment, the denitrification biofilter operated stably for 6 h, the carbon to nitrogen ratio was 4:1, and the hydraulic load was 2.0 $m^3/(m^2\ h)$. The carbon source types we tested were anhydrous sodium acetate, glucose, absolute ethanol, and methanol. We also tested the system without a carbon source. Denitrification was quantified based on the effluent from the filter column was measured, and the characteristics of each carbon source were analyzed and discussed. Each carbon source experiment was repeated twice, and the results were averaged. The operation was stable for three days after each carbon source replacement.

Fourth, we studied the effects of backwash on the denitrification performance of the DNBF. In this experiment, the external carbon source was anhydrous sodium acetate, the carbon to nitrogen ratio was 3.5:1, and the hydraulic load was 2.0 $m^3/(m^2\ h)$. In this phase, only water was used for flushing. The backwashing cycle was about 10 d, and the backwashing intensity was 10 $L/(m^2\ s)$. The state of recovery of the denitrification efficiency was measured 2, 4, 6, and 8 h after the DNBF was re-run. The shortest DNBF recovery time was identified.

Fifth, we investigated the effects of intermittent operation on DNBF denitrification performance. In this experiment, the external carbon source was anhydrous sodium acetate, the carbon to nitrogen ratio was 3.5:1, and the hydraulic load was 2.0 $m^3/(m^2\ h)$. The discontinuation time was 3 d and 15 d, and recovery was measured at 2, 4, 6, 8, and 10 h after the DNBF operation concluded.

2.6. Kinetic biological denitrification models of the DNBF

As the DNBF reaction progresses, the living microbial community inhabiting the reactor becomes particularly complicated [25]. For example, as the impurities trapped by the DNBF filter material gradually increased, the biofilm on the surface of the filter material thickened. This affected the motion of the water stream and might cause back mixing and axial mixing in severe cases [26]. Also, a very small amount of DO enters the denitrification filter along with the raw water, increasing the growth of nitrifying bacteria and aerobic denitrifying bacteria [27].

Given the complexity of the denitrification process, the model we designed was based on four assumptions. First, we assumed that the DNBF was an ideal push-flow reactor, without interior back mixing or axial mixing. Second, we assumed that the denitrification process only involved the microorganisms adsorbed on the surface of the filter material and that the effects of the microorganisms suspended in the filter tank are negligible. In addition, we assumed that the filter tank influent and effluent were both free of microorganisms. Third, we assumed that the entire filter was stable, with no accumulation of excess material, and that the removal amount was equal to the difference between the input amount and the output amount. Fourth, we assumed that the denitrification reaction occurred completely within the DNBF and that only denitrifying bacteria grew on the filter biofilm.

A simplified biological denitrification model is shown in Fig. 2. Given a microelement of volume V, the relationship between the concentration of NO_3^-–N in the filter and the height h of the filter layer was derived using Eq. (1).

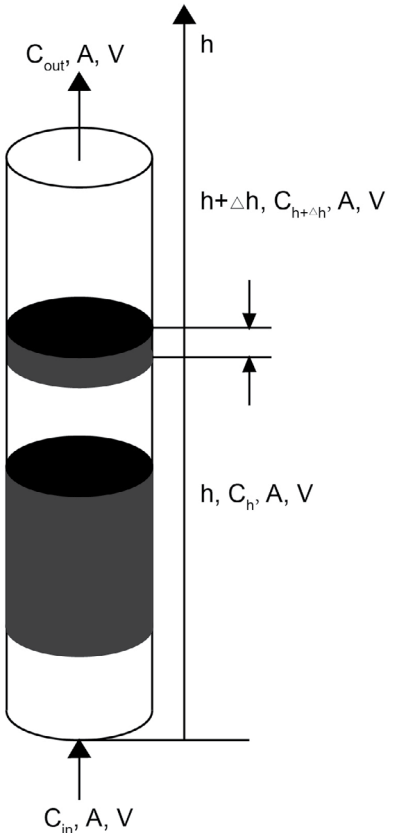

Fig. 2. Kinetic model of denitrification in denitrifying filter.

$$dV = A\mathrm{dh} \tag{1}$$

where dV was the volumetric micro-element of the filter layer; dh was the height of the filter layer, and A was the cross-sectional area of the filter layer (m^2).

Under stable conditions, the NO_3^-–N material balance analysis of NO_3^-–N was used to obtain Eqs. (2) and (3).

$$QdC_{NO_3} = rdV \tag{2}$$

$$\frac{dC_{NO_3}}{dh} = r\frac{A}{Q} \tag{3}$$

where Q was the influent flow rate (m^3/h); r was the denitrification reaction rate of the biofilm in the micro-element ($mgNO_3^-$–N/L h); and dC_{NO_3} was the change in nitrate concentration in and out of the micro-element (mg/L).

When the kinetic formula (Eq. (4)) was combined with the denitrification kinetic formula for the zero-order reaction (Eq. (5)), we obtained the 1/2-stage reaction (Eq. (6)) and the first-order reaction (Eq. (7)).

$$\frac{dC}{dt} = kC^a \tag{4}$$

where C was the concentration of NO_3^-N (mg/L); t was the hydraulic retention time (h); k was the reaction rate constant

(which was related to the filter material, the influent substrate concentration, and the mass transfer rate); and a was the number of reaction stages.

If the denitrification reaction is a zero-order reaction, $r = k_0$ and the formula for denitrification kinetics is:

$$\frac{dC_{NO_3}}{dh} = k_0 \frac{A}{Q} \tag{5}$$

If the denitrification reaction is a 1/2-stage reaction, $r = k_{1/2}C^{1/2}$ and the formula for denitrification kinetics is:

$$\frac{dC_{NO_3}^{\frac{1}{2}}}{dh} = k_{\frac{1}{2}} \frac{A}{Q} \tag{6}$$

If the denitrification reaction is a first-order reaction, $r = k_1C$ and the formula for denitrification kinetics is:

$$\frac{d\left(\ln C_{NO_3}\right)}{dh} = k_1 \frac{A}{Q} \tag{7}$$

3. Results and discussion

3.1. Characteristics of the ACLC

The dry density of the ACLC was 0.69 g/cm^3, and the wet density (after water absorption) was 0.87 g/cm^3. ACLC had a specific surface area of 13.6 g/m^2, an average particle size of 7 mm, and a particle size distribution of 6 mm. These data indicated that the ACLC was a suitable filter material. The low density of ACLC allowed it to float on water.

The SEM images of the ACLC before use (Figs. 3a and b) show that the ACLC surface was uneven and not tightly wrapped, with many unconnected, honeycombed micropores. This structure was due to the addition of a pore former, which makes the density of ACLC close to that of water, and allows ACLC to float above the water surface. The structure also indicated that the prepared ACLC had a high porosity and was suitable for use as a biological medium in the DNBF. The SEM images of the ACLC after use (Figs. 3c and d) show that biofilms contained many microorganisms; many cocci and bacilli were immobilized on the inner and outer surfaces of the ACLC pores. We observed this phenomenon at 5,000× magnification. At 8,000× magnification, it was clear that the tiny filaments were associated with each other, making the biofilm viscous.

Few absorption peaks in the infrared spectrum were identified by the FT-IR analysis of the ACLC (Fig. 3e). Thus, the composition of the ACLC was not complicated. The strongest absorption peak of ACLC (at 1,028.85 cm^{-1}) is the stretching vibration absorption peak of Si–O [28]. Thus, silica was the most abundant element in the ACLC. The second strong absorption peak of ACLC (at 473.59 cm^{-1}) was the absorption peak of Mg–O–Si. Therefore, ACLC also contained a large amount of magnesium silicate minerals. The peak at 3,432.59 cm^{-1} was the –OH stretching vibration absorption peak of crystal water [29].

3.2. Hanging of the biofilm and beginning operation

Denitrifying bacteria gradually become the dominant taxa during the DNBF operation. These bacteria form a denitrifying biofilm on the surface of the filter material [30]. The formation of the denitrifying biofilm was divided into two parts: the adaptation stage and the rapid propagation stage (Fig. 4a). The TN and NO_3^-–N removal rates increased slowly over the first 1–4 d. The average removal rate of TN was only 15%, and the average removal rate of nitrate-nitrogen was less than 5%. The low removal efficiency was because the operation of the entire device has just begun, and the denitrifying biofilm has not yet grown completely on the surface of the filter material. Thus, the reactor was mainly relying on the denitrifying bacteria suspended in the filter column to remove impurities. From day 5, the TN and NO_3^-–N removal rates increased rapidly. At this time, the denitrifying bacteria in the device are very active, multiplying rapidly, and looking for a suitable attachment medium. From day 16, the removal rate of TN reached 75%, and the

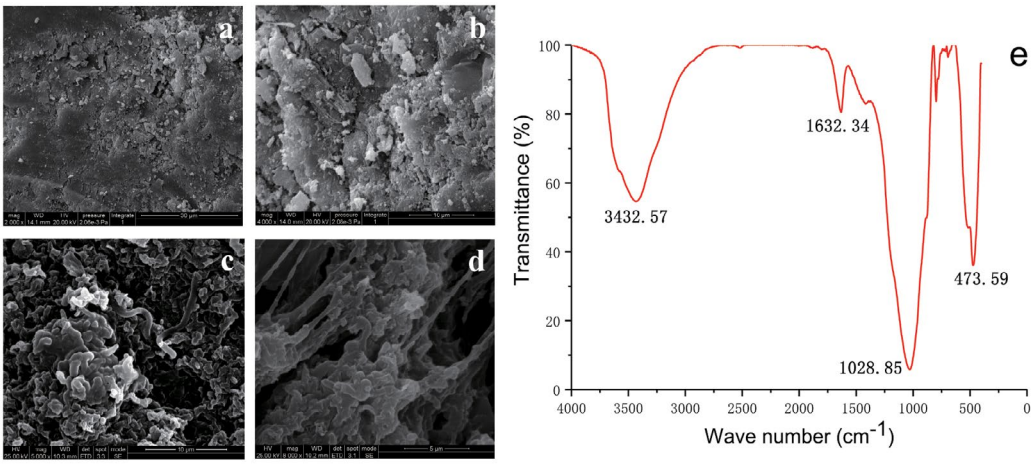

Fig. 3. (a) SEM image of ACLC before use at 2,000×, (b) SEM image of ACLC before use at 4,000×, (c) SEM image of ACLC after use at 5,000×, (d) SEM image of ACLC after use at 8,000×, and (e) FT-IR spectra of ACLC.

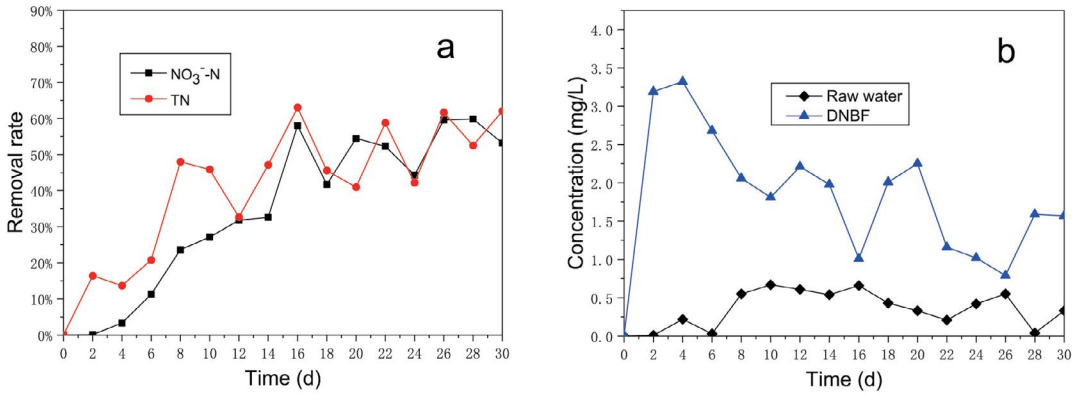

Fig. 4. (a) Removal of TN and NO_3^-–N once the film was hung and (b) change in NO_2^-–N concentration after the film was hung.

removal rate of NO_3^-–N reached 60%. By this time, a biofilm had formed on the surface of the filter material, and many bubbles were observed through the glass filter column; the bubbles were redox-formed nitrogen [31]. Thus, we concluded that by day 16, all three columns were successfully filmed. There was a significant decline in the removal rate after 16 d. This was because the DNBF was backwashed, decreasing the biomass of the filter surface. The DNBF was continuously operated for an additional 10 d. Removal continued slowly after 16 d. This indicated that the DNBF still had a certain denitrification potential.

The concentration of NO_2^-–N in the raw water was compared to that in the DNBF effluent (Fig. 4b). Nitrite is an intermediate product of the oxidation and reduction of NO_3^-–N to nitrogen under the action of denitrifying bacteria. The higher nitrate concentration, the less complete the redox. NO_2^-–N was produced in the raw water because a very small portion of the nitrate in the water was reduced to nitrite upon exposure to air [32]. The initial NO_2^-–N concentration in the DNBF was very high because the amount of denitrifying bacteria or NO_2^-–N reductase was insufficient. Thus, NO_2^-–N was not completely reduced, resulting in a sizeable accumulation of NO_2^-–N [33]. After the biofilm was hung, the denitrifying biofilm had formed and NO_2^-–N accumulation had decreased significantly. After successful filming, the NO_2^-–N concentration in the DNBF was 1 mg/L.

3.3. Effects of hydraulic load

In general, the smaller the hydraulic load in the denitrification filter (i.e., the longer the hydraulic retention time), the better the denitrification effect [13]. However, if the hydraulic load is too small, the water flow rate will be slow, the running time will be too long, and the economic cost will increase [34]. Therefore, in these experiments we aimed to identify optimal running conditions, yielding a good level of denitrification with a moderate hydraulic load. As hydraulic load increased, the removal effect of TN and NO_3^-–N gradually decreased (Figs. 5a and b). When the hydraulic load was 7.0 $m^3/(m^2\ h)$, the DNBF removal rates of TN and nitrate nitrogen were 10% and 9%, respectively. That was because increased hydraulic loads increase water flow rates, reducing the amount of time that the raw water can react with the denitrifying biofilm and decreasing the efficacy of the reaction. The denitrification performance of the filter material indicated that either 1.4 or 2.0 $m^3/(m^2\ h)$ was the optimal hydraulic load. Based on economic factors and the decontamination cycle, we chose 2.0 $m^3/(m^2\ h)$ as the optimal hydraulic load for this experiment. Under this hydraulic load, the removal rate of TN and NO_3^-–N gradually increased with the height of the filter layer. When the hydraulic load was 2.0 $m^3/(m^2\ h)$, the removal efficiencies of TN and nitrate nitrogen by the light filter column were 81% and 88%, respectively. The pollutant removal effects were most obvious with filter layers 0–20 cm in height: at these heights, the maximum removal rate of TN and NO_3^-–N was 80%. This was because the denitrifying bacteria were most active in filter columns 0–20 cm high. When the raw water entered the DNBF, the concentration of nitrogen compounds was high, supplying sufficient nutrients to allow the denitrifying biofilm to grow vigorously. Thus, both the denitrification rate and the decontamination performance of the DNBF were high.

When the hydraulic load was 1.4 and 2.0 $m^3/(m^2\ h)$, the concentration of NO_2^-–N decreased with increased filter layer height (Fig. 5c). At hydraulic loads of 1.4 and 2.0 $m^3/(m^2\ h)$, the DNBF effluent concentrations were 0.086 and 0.52 mg/L, respectively. At hydraulic loads of 3.0–7.0 $m^3/(m^2\ h)$, NO_2^-–N accumulation increased with the height of the filter layer, up to a maximum concentration of 4.12 mg/L. This was because, as the hydraulic load increased, the water flow rate gradually increased, and nitrate reduction decreased. At a hydraulic load of 3.0 $m^3/(m^2\ h)$, the nitrate reduction rate exceeded the nitrite reduction rate. As the height of the filter layer increased, the reaction progressed and nitrite accumulation increased. In addition, the TN removal rate was low due to the high NO_2^-–N content.

As filter layer height increased, pH increased as well; pH was highest at a filter layer height of 0–20 cm (Fig. 5d). This was because denitrification was accompanied by the production of alkaline substances, which led to an increase in the pH of DNBF. Denitrifying bacteria are most active at 0–20 cm [35]. Also, the greater the hydraulic load, the smaller the pH change. When the hydraulic load was 6.0 or 7.0 $m^3/(m^2\ h)$, the pH did not change substantially, because at greater hydraulic loads, less organic matter is consumed and less alkaline material is produced [36].

DO concentration gradually decreased as the filter layer increased; this decrease was most obvious at heights of

0–20 cm (Fig. 6a). At these filter layer heights, sufficient organic matter and nutrients were present, as well as aerobic microorganisms. Thus, oxygen was rapidly decomposed to produce carbon dioxide and energy for microbes. The greater the hydraulic load, the faster the water flow rate; this decreases the amount of oxygen bound by organic matter and increases DO concentration [5]. With the same hydraulic load, although DO primarily decreased with filter layer height, DO increase slightly at a certain filter height, possible because microorganisms use nitrogen as a nitrogen source, and cause the assimilation of nitrate reduction [37]. Moreover, the conversion of nitrate-nitrogen to ammonia nitrogen releases a small amount of oxygen.

3.4. Effects of carbon to nitrogen ratio

During the denitrification process, the carbon source acts as an electron donor. The carbon source not only provides electrons for the redox oxidation of NO_2^-–N to nitrogen, but also for the production of new products [38]. If the carbon source load is too low, denitrification will be insufficient, and the denitrification effect will not be obvious [39]. However, increasing the carbon source load increases the cost of the reaction. It is also important that effluent organic matter content is below the discharge standard [40]. Thus, it is critical to identify the optimal carbon to nitrogen ratio. As the carbon to nitrogen ratio increased, the removal rates of TN and NO_3^-–N by the DNBF also increased (Figs. 6b and c). At a carbon to nitrogen ratio of 4:1, the maximum TN and NO_3^-–N removal rates were observed (85% and 91%, respectively). This may have been because, at this ratio, the carbon source was sufficient. In addition, the organic matter decomposed, releasing energy. These factors may have enhanced the activity of the denitrifying bacteria and increased the denitrification reaction. When the carbon to nitrogen ratio was increased from 4:1 to 4.5:1, the TN and NO_3^-–N removal rates decreased by about 5%. This may have been because the experimental equipment had a carbon to nitrogen ratio of 3.5:1 set at the beginning of the startup period. The sudden increase in carbon source concentration may have led to the rejection of denitrifying bacteria in the reactor. In addition, if the carbon source concentration is too high, the organic matter that the denitrifying bacteria cannot consume will be absorbed by other heterotrophic bacteria, which will grow and eventually inhibit the activity of denitrifying bacteria [41]. At the same carbon to nitrogen ratio, the removal rates of TN and NO_3^-–N is increased as the reaction progressed, especially for low carbon to nitrogen ratios. This may have been because the carbon source concentration was low, the energy released by the decomposition of organic

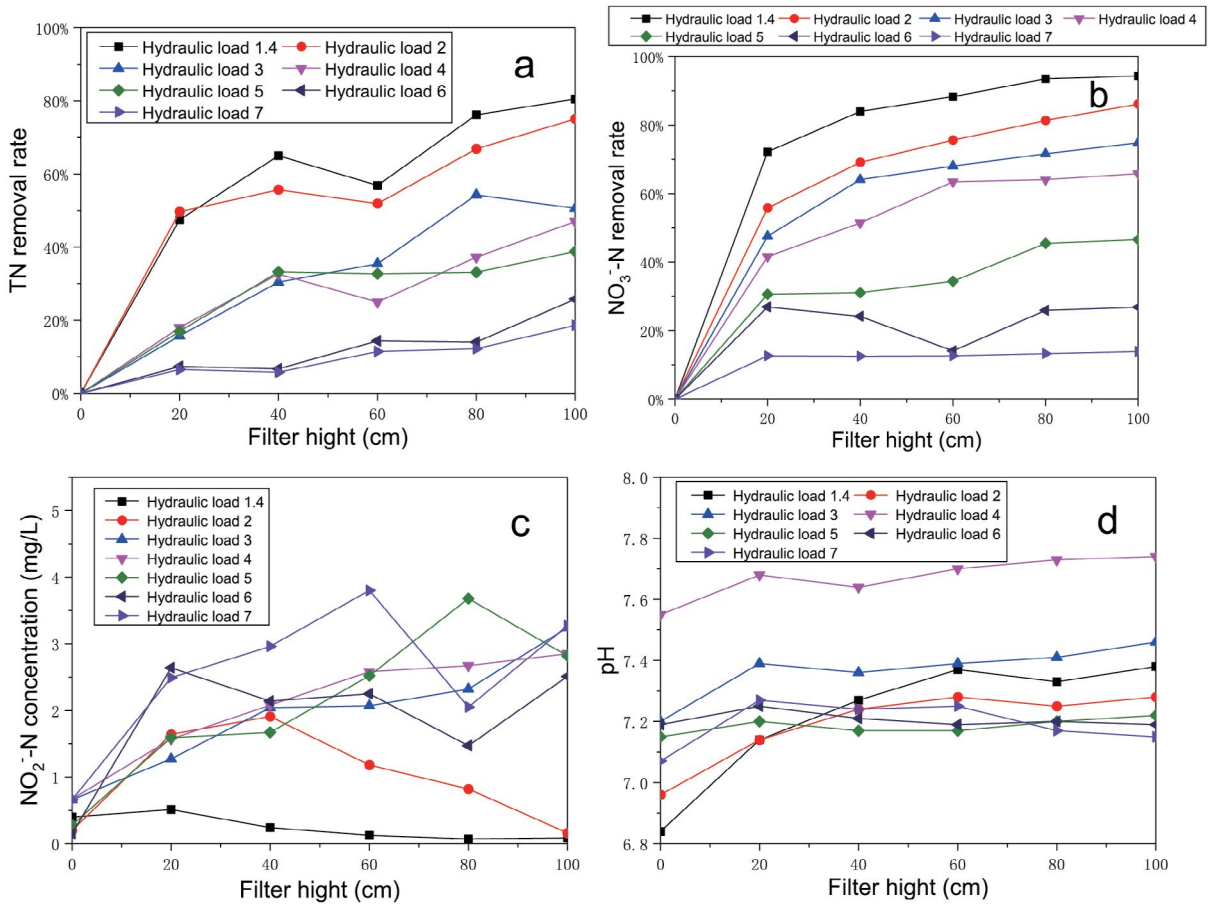

Fig. 5. (a) TN removal rate under different hydraulic loads and column height, (b) NO_3^-–N removal rate under different hydraulic loads and column height, (c) NO_2^-–N concentration under different hydraulic loads and column height, and (d) Variation of pH value at different hydraulic loads and column height.

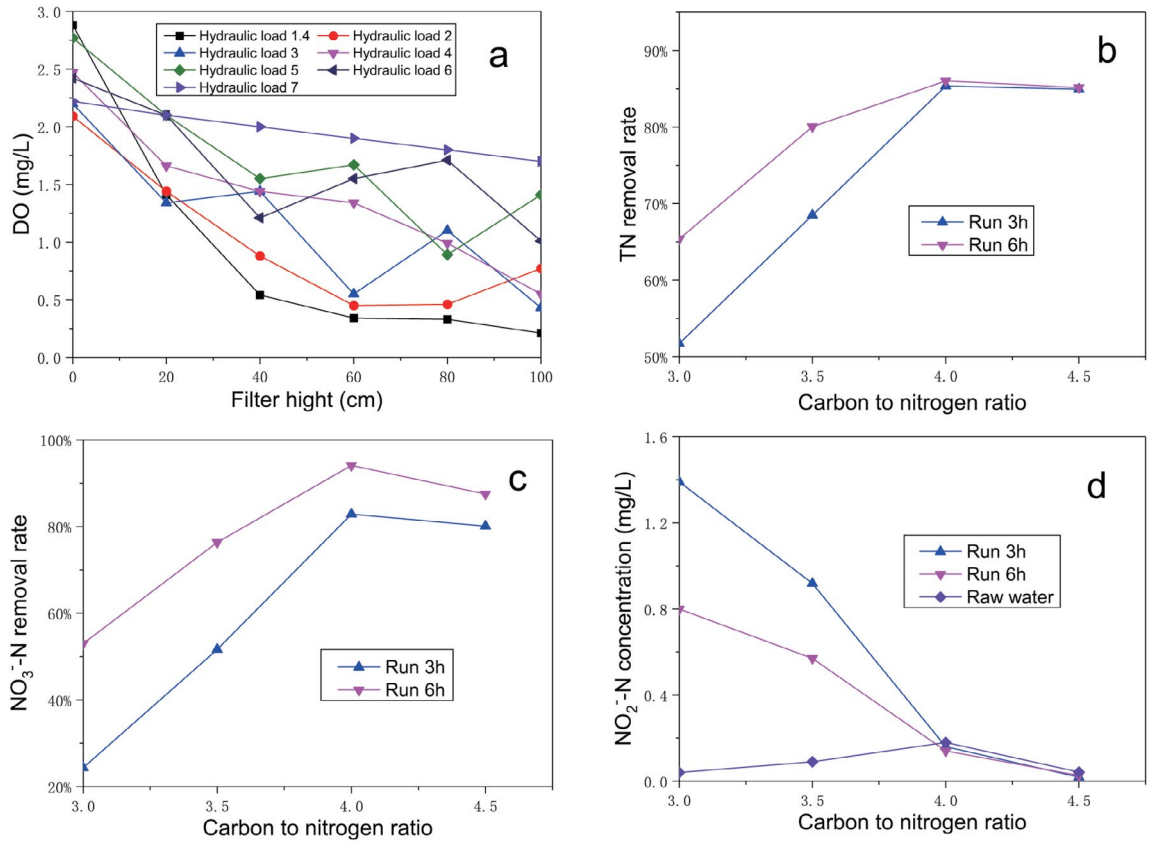

Fig. 6. (a) Variations in DO at different hydraulic loads and column heights, (b) TN removal rate at different carbon/nitrogen ratios, (c) NO_3^-–N removal rate at different carbon/nitrogen ratios, and (d) changes in NO_2^-–N concentration at different carbon/nitrogen ratios.

matter was low, and microbial activity was low; thus, denitrification was not thorough. The carbon source would be better spread through long-term operation [42].

The concentration of NO_2^-–N decreased gradually as the carbon to nitrogen ratio increased (Fig. 6d). At carbon to nitrogen ratios of 4:1 and 4.5:1, the concentration of NO_2^-–N in the DNBF was lower than that in the raw water. This was because the carbon source concentration was insufficient, and thus denitrification remains at the nitrosation stage. As the concentration of the carbon sources increases, denitrification proceeds more thoroughly [43].

3.5. Effects of carbon source

The same filter materials have different denitrification effects on different carbon sources. Each filter has the most suitable type of carbon source [44]. When sodium acetate and ethanol were used as carbon sources, the denitrification effect was significantly greater than when methanol, glucose, and internal carbon sources were used (Figs. 7a and b). This was because sodium acetate and ethanol have high biological activity and quickly reacted with the pollutants entering the reaction vessel [5]. Thus, the denitrification rate was extremely high. Most microorganisms in denitrification filters use glucose to synthesize cytoplasm and to release energy for anabolism [43]. Therefore, the glucose was primarily used for cell synthesis, and little of the glucose was used for denitrification. The cumulative amount of NO_2^-–N was greatest when the carbon source was internal, followed by sodium acetate, methanol, ethanol, and glucose (Fig. 7c). When an internal carbon source was used, NO_2^-–N accumulation was high because the reaction was insufficient. When sodium acetate was used, NO_2^-–N accumulation was high due to differences in its specific metabolic pathways [45].

3.6. Effects of backwash

Backwashing is an indispensable step in DNBF operation, which effectively guarantees DNBF processing power [44]. According to biofilm formation theory, bacteria initially form a non-specific and reversible attachment to the surface of the filter material. When the attachment becomes permanent, the bacteria begin to synthesize insoluble exopolysaccharides, which enclose the colonies of adherent bacteria. As insoluble exopolysaccharides accumulate and bacteria proliferate, colonies develop into mature biofilms [46]. When the high-speed water stream rinses the denitrification filter column, the filter material in the filter column flows and collides together. At this time, most of the old biofilms are detached by rinsing and discharged along with the water. As wastewater is re-filtered in DNBF, a new biofilm growth cycle is

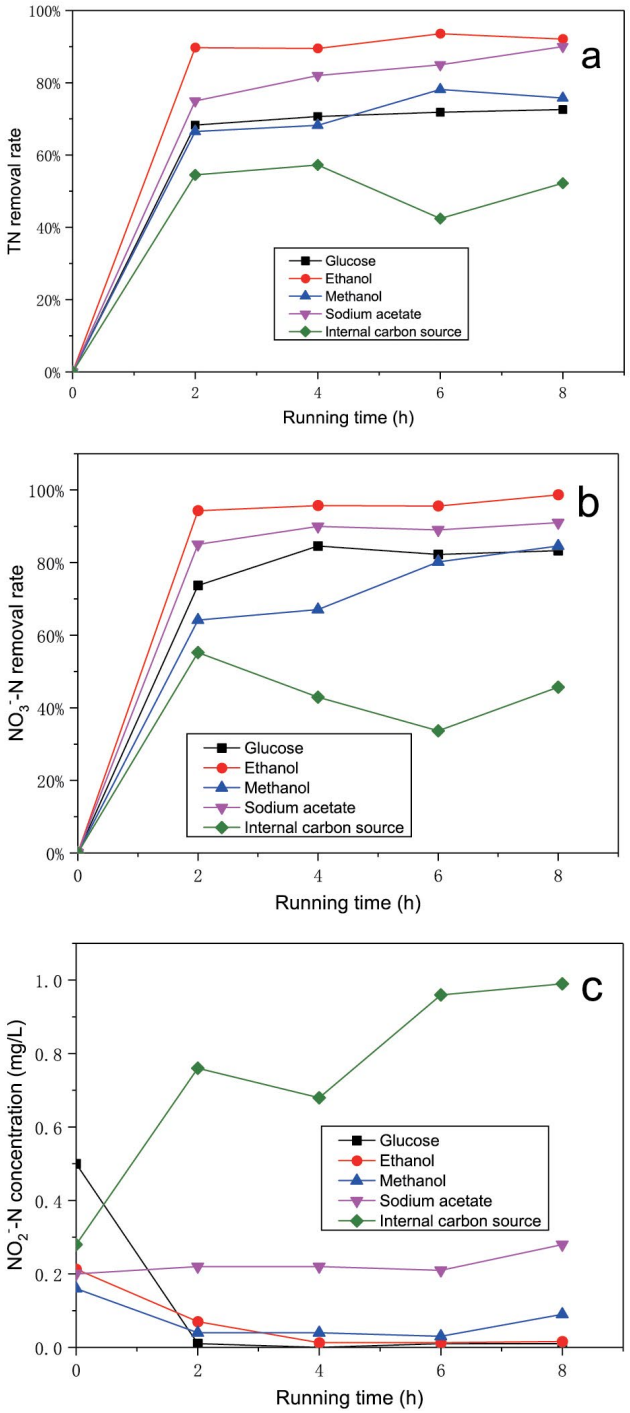

Fig. 7. (a) TN removal rate under different carbon sources, (b) NO_3^-–N removal rate under different carbon sources, and (c) Variation of NO_2^-–N concentration in different carbon sources.

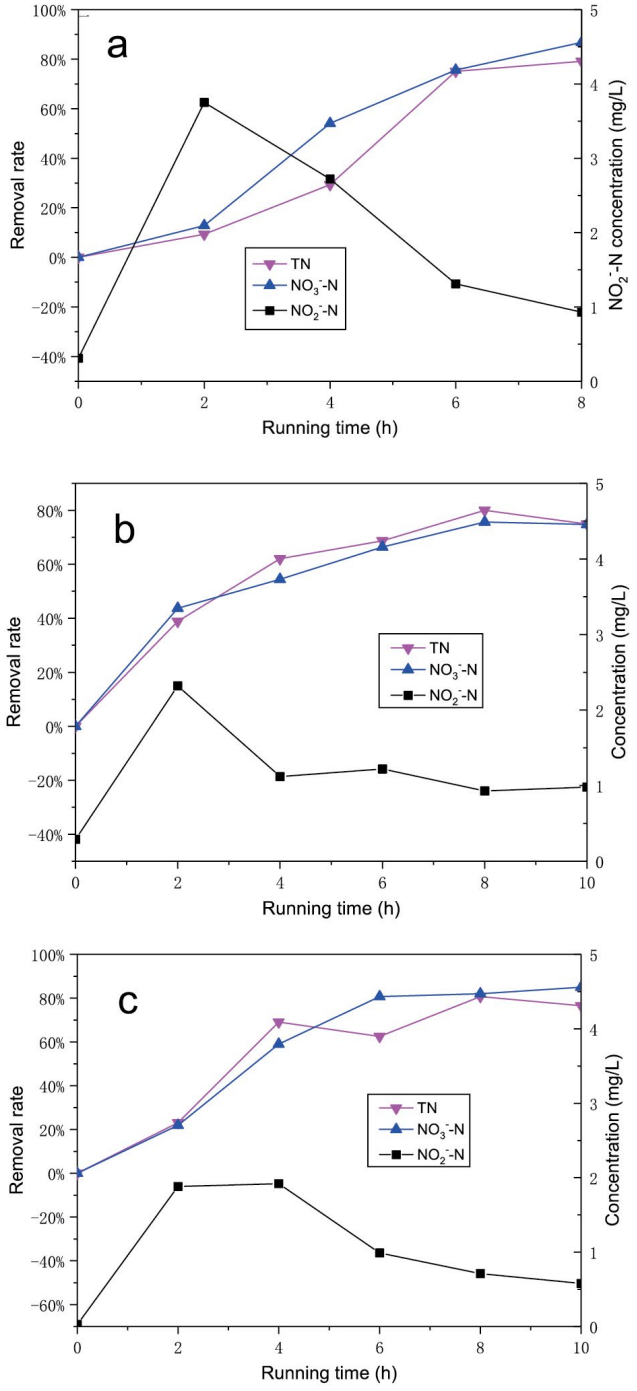

Fig. 8. (a) Recovery of DNBF after backwashing, (b) recovery of DNBF after 3 d, and (c) recovery of DNBF after 15 d.

restarted [38]. The concentration of NO_2^-–N increased from 0.31 to 3.75 mg/L within 2 h after backwashing (Fig. 8a). The removal rates of TN and NO_3^-–N by DNBF increased slowly. This is because the residual cells and microflora on the surface of filter media are replicated after backwashing, which makes NO_2^-–N accumulate during the growth of biofilm and plays an important role in nitrate removal [11]. The denitrification performance of DNBF recovered continuously between 2 and 6 h. At this time, the concentration of NO_2^-–N decreased sharply from 3.75 to 1.31 mg/L. The removal rates of TN and NO_3^-–N increased to 75% and 75.5% respectively. These results indicate that the growth of biofilm not only improves the removal rate of nitrate and TN but also reduces the nitrite produced during nitrate reduction. After 6 h, the removal rates of TN and NO_3^-–N tended to be

stable, reaching 79.1% and 86.7% respectively. This indicates that the new biofilm has grown steadily and the denitrification performance has been restored.

3.7. Effects of intermittent operation

The DNBF had a recovery period after the device was stopped (Figs. 8b and c). The concentration of NO_2^-–N in DNBF which shutdown of 3 d increased from 0.29 to 2.32 mg/L within 2 h after equipment restart. The removal rates of TN and NO_3^-–N showed an upward trend. This was because, while the device was non-operational, the denitrifying bacteria could not absorb sufficient nutrients. The bacteria thus began to die. As the denitrifying biofilm was not replaced, the denitrification rate decreased. When the equipment is re-run, the residual bacteria get nutrients and gradually resume their activity and reproduction. By contrast, the recovery of DNBF after 15 d of downtime is slower. This can be attributed to the fact that denitrifying bacteria have a higher mortality rate and take longer to recover from chronic undernutrition. After 8 h of restart, the denitrification performance of both DNBFs was restored, and the removal rates of TN and NO_3^-–N were above 79% and 75%. It may be that the aging process gradually slows after the reduction of denitrifying bacterial activity [47].

3.8. Biological denitrification kinetics of the DNBF

3.8.1. Determination of the kinetic parameters of biological denitrification

At the stage when the raw water entered the DNBF, the organic matter content in the liquid phase of the main body of the reactor was high due to both the carbon source and the high concentration of NO_2^-–N in the raw water. At this point, the mass transfer process might be considered a zero-order reaction. As the microbial content in the denitrifying biofilm on the filter material was limited, the biological denitrification reaction controlled the rate of the entire DNBF reaction. However, when sufficient denitrifying bacteria were present in the denitrifying biofilm, the denitrification reaction in the biofilm might be considered a zero-order reaction.

When the concentration of organic matter and nitrate in the liquid phase of the main body of the reactor was slightly reduced, the mass transfer process restricted the denitrification reaction of the entire DNBF. At this point, the mass transfer of organic matter or nitrate to the biofilm became a limiting factor for the denitrification reaction. The kinetic progression of the denitrification reaction of the entire DNBF could be considered one stage [26]. The actual denitrification process was affected by various factors and was between these two extremes. Therefore, the denitrification kinetics of the DNBF were between 1/2 and 1.

The DNBF was operated stably for 6 h, with a sodium acetate carbon source, carbon to nitrogen ratio of 3.5:1, and a hydraulic load of 2.0 $m^3/(m^2\ h)$. The obtained NO_3^-–N range concentration test data (Table 2) were used to simulate zero-order, 1/2-level, and first-order dynamic equations (Figs. 9a-c). The correlation coefficient (R^2) of the 1/2-order reaction was 0.946; the correlation coefficient (R^2) of the first-order reaction was 0.993, and the correlation coefficient (R^2) of the zero-order reaction was 0.849. Therefore, the

Table 2
Changes in NO_3^-–N concentration in the DNBF

Filter height (cm)	NO_3^-–N concentration (mg/L)
0	8.5
20	4.85
40	3.46
60	1.98
80	1.28
100	0.93

1/2-stage reaction and the first-order reaction fit the DNBF better than did the zero-order reaction. We can conclude that from the accuracy of the DNBF denitrification process, the first level > 1/2 level > zero level.

Based on our results, the denitrification first-order kinetic reaction model was further transformed (Eq. (8)).

$$C = 8.13e^{\left(\frac{kh}{v}\right)} \tag{8}$$

where h is the filter material height (cm), k is the kinetic constant (h^{-1}), and v is the filter speed (m/L).

K-values were obtained at different filtration rates (Table 3). The K-values at different filtration rates were fitted (Fig. 9d). The kinetic constant k had a strong linear relationship with the filtration rate v. As k is a linear function of v, the relationship between them can be expressed as Eq. (9). Thus, the kinetic equation for denitrification can be expressed as Eq. (10).

$$k = -0.0087\mathrm{V} - 0.0274 \tag{9}$$

$$C = 8.13e^{\left(\frac{(0.0087v-0.0274)h}{v}\right)} \tag{10}$$

3.8.2. Verification of the biological denitrification kinetic equation

The NO_3^-–N concentrations in the DNBF effluent under optimal operating conditions were used to verify the denitrification kinetics equations derived above. For this verification, sodium acetate was used as the carbon source, and the carbon to nitrogen ratio was set to 3.5:1. The experiment was performed five times. The simulated results, based on the derived formulae, were less than experimental results, but the relative error did not exceed 20% (Table 4). We thus concluded that the model formula roughly reflected the denitrification process under the existing water quality conditions. The experimental results differed from the calculated results, possibly due to mass transfer in the filter, the nature of the filter material, the biofilm, or the presence of simultaneous nitrification, denitrification and short-range denitrification inside the filter.

4. Conclusion

The ACLC preparation method described herein was simple and economical. ACLC had a rough surface and a

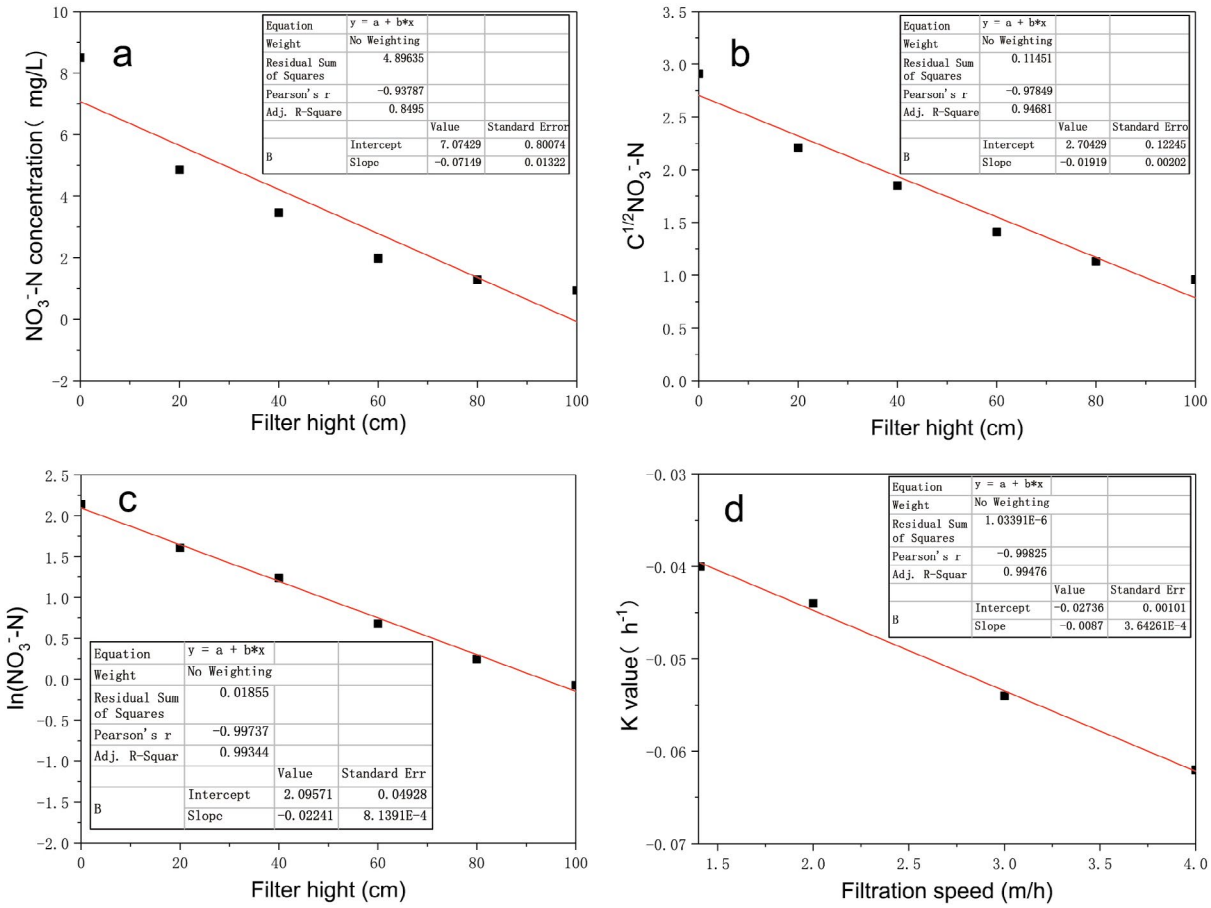

Fig. 9. (a) Fit of a zero-order reaction to the DNBF data, (b) fit of a half-order reaction to the DNBF data, (c) fit of a first-order reaction to the DNBF data, and (d) functional relationship between the kinetic constants and the DNBF filtration rate.

large number of unconnected honeycombed micropores. Therefore, bacteria adhered easily to this material, and biofilm formation was rapid. The ACLC density is close to the density of water and therefore can float on the water.

Table 3
K-values of the DNBF at different filtration speeds

Filtration speed (m/h)	*K*-value (h^{-1})
1.41	–0.04
2.0	–0.044
3.0	–0.054
4.0	–0.062

The ACLC DNBF effectively removed nitrogen from nitrogen-contaminated water. Our optimization experiments identified the following optimal DNBF conditions: a hydraulic load of 2.0 $m^3/(m^2\,h)$, a carbon to nitrogen ratio of 4:1, and an anhydrous sodium acetate carbon source. Under these optimal conditions, the removal rates of TN and NO_3^-–N were 87% and 90%, respectively. In addition, the accumulation of NO_2^-–N was reduced to 0.18 mg/L. The DNBF recovered rapidly (6 h) after backwash, 3 d outage, and 6 d stoppage. The biological denitrification kinetics of the DNBF indicated that the first-order reaction was most suitable for describing the DNBF denitrification process (correlation coefficient $R^2 = 0.993$). Therefore, it is cost-effective to treat nitrogen-contaminated water sources with an ACLC DNBF.

Table 4
Comparison of DNBF simulation and actual results

Factors	Sample 1	Sample 2	Sample 3	Sample 4	Sample 5
Actual value (mg/L)	4.56	3.39	1.96	5.41	3.04
Analog value (mg/L)	4.72	3.17	2.03	4.57	3.78
Relative error (%)	3.4	6.4	2.5	15.5	19.6

Acknowledgments

The authors express their sincere gratitude to the National Natural Science Foundation of China (51608272), the Postgraduate Research &Practice Innovation Program of Jiangsu Province (KYCX18_0973), the Science and Technology Project of Jiangsu Provincial Department of Housing and Urban-Rural Development (2017ZD055) and a project funded by the Priority Academic Program Development of the Jiangsu Higher Education Institutions (PAPD) for financial support.

References

[1] Y.L. Wang, S. Xue, H.B. Wang, X.X. Xu, B.Z. Liu, W.H. Wang, F. Xu, J.Q. Jia, Characteristics of nitrogen removal and sludge reduction using a multi-redox environment coupled bioreactor, Desal. Wat. Treat., 132 (2018) 89–98.
[2] Z.Q. Dai, X.W. Lu, Z.Q. Jing, Nitrogen and phosphorus removal processes under different aeration strengths in the principal-type tank of alternate multiple tanks system and process control, Environ. Technol., 40 (2019) 489–498.
[3] Y.Q. Li, W.J. Yan, F. Wang, S.C. Lv, Q.Q. Li, Q.B. Yu, Nitrogen pollution and sources in an aquatic system at an agricultural coastal area of Eastern China based on a dual-isotope approach, Environ. Sci. Pollut. Res., 26 (2019) 23807–23823.
[4] Y. Zhang, P. Shi, J. Song, Q. Li, Application of nitrogen and oxygen isotopes for source and fate identification of nitrate pollution in surface water: a review, Appl. Sci. Basel, 9 (2019) 18.
[5] N. Wei, Y.H. Shi, G.X. Wu, H.Y. Hu, Y.H. Wu, H. Wen, Tertiary denitrification of the secondary effluent by denitrifying biofilters packed with different sizes of quartz sand, Water, 6 (2014) 1300–1311.
[6] Y.L. Wang, B.Z. Liu, K.F. Zhang, Y.J. Liu, X.X. Xu, J.Q. Jia, Investigate of in situ sludge reduction in sequencing batch biofilm reactor: performances, mechanisms and comparison of different carriers, Front. Environ. Sci. Eng., 12 (2018) 5.
[7] Y.L. Wang, J. Li, W.J. Jia, N. Wang, H.B. Wang, S. Zhang, G.H. Chen, Enhanced nitrogen and phosphorus removal in the A_2/O process by hydrolysis and acidification of primary sludge, Desal. Wat. Treat., 52 (2014) 5144–5151.
[8] Y.G. Ren, J.H. Wang, H.F. Li, J. Zhang, P.Y. Qi, Z. Hu, Nitrous oxide and methane emissions from different treatment processes in full-scale municipal wastewater treatment plants, Environ. Technol., 34 (2013) 2917–2927.
[9] X. Liu, H. Wang, F. Long, L. Qi, H. Fan, Optimizing and real-time control of biofilm formation, growth and renewal in denitrifying biofilter, Bioresour. Technol., 209 (2016) 326–332.
[10] C. Du, C.W. Cui, S. Qiu, S.N. Shi, A. Li, F. Ma, Nitrogen removal and microbial community shift in an aerobic denitrification reactor bioaugmented with a *Pseudomonas* strain for coal-based ethylene glycol industry wastewater treatment, Environ. Sci. Pollut. Res., 24 (2017) 11435–11445.
[11] B. Cui, X. Liu, Q. Yang, J. Li, X. Zhou, Y. Peng, Achieving partial denitrification through control of biofilm structure during biofilm growth in denitrifying biofilter, Bioresour. Technol., 238 (2017) 223–231.
[12] Z.Q. Jing, R. He, Y. Hu, Q.G. Niu, S.W. Cao, Y.Y. Li, Practice of integrated system of biofilter and constructed wetland in highly polluted surface water treatment, Ecol. Eng., 75 (2015) 462–469.
[13] Z. Wang, Z.J. Wang, L. Chen, Z.Z. Lin, Y.L. Liu, Y. Liu, Using an attapulgite-activated carbon composite ceramisite biofilter to remove dibutyl phthalate from source water, Pol. J. Environ. Stud., 27 (2018) 897–903.
[14] M. Lu, G.H. Xia, X.D. Zhao, Surface modification of porous suspended ceramsite used for water treatment by activated carbon/Fe_3O_4 magnetic composites, Environ. Technol., 34 (2013) 2301–2307.
[15] Z.Q. Jing, Y.Y. Peng, R. He, Y. Xu, T. Yu, J. Hu, Poplar leaves reclamation for porous granules and their application in nitrobenzene removal from aqueous solution, Desal. Wat. Treat., 57 (2016) 449–458.
[16] D.T. Yue, Q.Y. Yue, B.Y. Gao, H.T. He, H. Yu, S.L. Sun, Q. Li, Y. Wang, Y. Zhao, Preparation and bloating mechanism of porous ultra-lightweight ceramsite by dehydrated sewage sludge and Yellow River sediments, J. Wuhan. Univ. Technol., 29 (2014) 1129–1135.
[17] K. Nurk, I. Zaytsev, I. Talpsep, J. Truu, U. Mander, Bioaugmentation in a newly established LECA-based horizontal flow soil filter reduces the adaptation period and enhances denitrification, Bioresour. Technol., 100 (2009) 6284–6289.
[18] S.H. Lin, T.T. Zhou, S.S. Yin, Properties of thermally treated granular montmorillonite palygorskite adsorbent (GMPA) and use to remove Pb^{2+} and Cu^{2+} from aqueous solutions, Clays Clay Miner., 65 (2017) 184–192.
[19] L. Hlungwane, E.L. Viljoen, V.E. Pakade, Macadamia nutshells-derived activated carbon and attapulgite clay combination for synergistic removal of Cr(VI) and Cr(III), Adsorpt. Sci. Technol., 36 (2017) 713–731.
[20] Z.Q. Jing, Characterization of nanoporous ceramic granules made with coal fly ash and their utilization in phenol removal from water, J. Nanomater., 2013 (2013) 8 p, http://dx.doi.org/10.1155/2013/606940.
[21] B. Sun, H. Wang, C.F. Ding, Y.X. Guo, S.G. Zhu, J. Zhang, L.T. Kong, Preparation and evaluation of granular Fe-impregnated attapulgite adsorbents (Fe-ATP) for arsenic removal from contaminated groundwater, Desal. Wat. Treat., 141 (2019) 256–268.
[22] J. Tang, L. Zong, B. Mu, Y.R. Kang, A.Q. Wang, Attapulgite/carbon composites as a recyclable adsorbent for antibiotics removal, Korean J. Chem. Eng., 35 (2018) 1650–1661.
[23] G. Liu, Z. Li, L. Xu, X. Xu, Q. Huang, Y. Zeng, M. Wen, The dynamics and adsorption of Cd(II) onto hydroxyapatite attapulgite composites from aqueous solution, J. Sol-Gel Sci. Technol., 87 (2018) 269–284.
[24] T.Y. Xie, Z.Q. Jing, J. Hu, P. Yuan, Y.L. Liu, S.W. Cao, Degradation of nitrobenzene-containing wastewater by a microbial-fuel-cell-coupled constructed wetland, Ecol. Eng., 112 (2018) 65–71.
[25] V. Evrard, R.N. Glud, P.L.M. Cook, The kinetics of denitrification in permeable sediments, Biogeochemistry, 113 (2013) 563–572.
[26] V.L. Mathioudakis, A. Aivasidis, Heterotrophic denitrification kinetics in a pressurized sewer biofilm reactor, Desalination, 248 (2009) 696–704.
[27] M.L. McCrackin, J.J. Elser, Denitrification kinetics and denitrifier abundances in sediments of lakes receiving atmospheric nitrogen deposition (Colorado, USA), Biogeochemistry, 108 (2011) 39–54.
[28] L. Nemes, E.E. Brown, C.S.-C. Yang, U. Hommerich, Mid infrared emission spectroscopy of carbon plasma, Spectrochim. Acta, Part A, 170 (2017) 145–149.
[29] K.M. Tan, G.P. Singh, C.S. Herrington, C.T.A. Brown, Near-infrared Raman spectroscopy using hollow-core photonic bandgap fibers, Opt. Commun., 283 (2010) 3204–3206.
[30] V. Geoffroy, G. Payette, F. Mauffrey, L. Lestin, P. Constant, R. Villemue, Strain-level genetic diversity of *Methylophaga nitratireducenticrescens* confers plasticity to denitrification capacity in a methylotrophic marine denitrifying biofilm, PeerJ, 6 (2018) e4679.
[31] B. Moreno, M.A. Gomez, A. Ramos, J. Gonzalez-Lopez, E. Hontoria, Influence of inocula over start up of a denitrifying submerged filter applied to nitrate contaminated groundwater treatment, J. Hazard. Mater., 127 (2005) 180–186.
[32] L. Guo, Y.D. Guo, M. Sun, M.C. Gao, Y.G. Zhao, Z.L. She, Enhancing denitrification with waste sludge carbon source: the substrate metabolism process and mechanisms, Environ. Sci. Pollut. Res., 25 (2018) 13079–13092.
[33] X. Ji, Y. Liu, J. Zhang, D. Huang, P. Zhou, Z. Zheng, Development of model simulation based on BioWin and dynamic analyses on advanced nitrate nitrogen removal in deep bed denitrification filter, Bioprocess. Biosyst. Eng., 42 (2018) 199–212.
[34] M. Seres, K.A. Mocova, J. Moradi, M. Kriska, V. Koci, T. Hnatkova, The impact of woodchip-gravel mixture on the efficiency and toxicity of denitrification bioreactors, Sci. Total Environ., 647 (2019) 888–894.

[35] M. Raboni, V. Torretta, A modified biotrickling filter for nitrification-denitrification in the treatment of an ammonia-contaminated air stream, Environ. Sci. Pollut. Res., 23 (2016) 24256–24264.
[36] Z. Zhang, Z.W. Hao, Y.P. Yang, J.H. Zhang, Q. Wang, X.H. Xu, Reductive denitrification kinetics of nitrite by zero-valent iron, Desalination, 257 (2010) 158–162.
[37] S.L. Zhou, Y.R. Zhang, T.L. Huang, Y.F. Liu, K.K. Fang, C.H. Zhang, Microbial aerobic denitrification dominates nitrogen losses from reservoir ecosystem in the spring of Zhoucun reservoir, Sci. Total Environ., 651 (2019) 998–1010.
[38] Z. Wang, M.G. Zhong, J.F. Wan, G.J. Xu, Y. Liu, Development of attapulgite composite ceramsite/quartz sand double-layer biofilter for micropolluted drinking source water purification, Int. J. Environ. Sci. Technol., 13 (2016) 825–834.
[39] H.S. Fowdar, B.E. Hatt, P. Breen, P.L. Cook, A. Deletic, Evaluation of sustainable electron donors for nitrate removal in different water media, Water Res., 85 (2015) 487–496.
[40] Y.Q. Wu, K. Song, Y.H. Jiang, X.Y. Sun, L. Li, Effect of thermal hydrolysis sludge supernatant as carbon source for biological denitrification with pilot-scale two-stage anoxic/oxic process and nitrogen balance model establishment, Biochem. Eng. J., 139 (2018) 132–138.
[41] H.Y. Zheng, Y. Liu, X.Y. Gao, G.M. Ai, L.L. Miao, Z.P. Liu, Characterization of a marine origin aerobic nitrifying-denitrifying bacterium, J. Biosci. Bioeng., 114 (2012) 33–37.
[42] E.C. Li, X.W. Jin, S.G. Lu, Microbial communities in biological denitrification system using methanol as carbon source for treatment of reverse osmosis concentrate from coking wastewater, J. Water Reuse Desal., 8 (2018) 360–371.
[43] L. Wang, J.Q. Tian, Y.M. Li, Nitrite accumulation and nitrous oxide emission during denitrification processes with quinoline or indole as the sole carbon source, J. Chem. Technol. Biotechnol., 90 (2015) 1317–1328.
[44] F. Yan, J.G. Jiang, H.W. Zhang, N. Liu, Q. Zou, Biological denitrification from mature landfill leachate using a food-waste-derived carbon source, J. Environ. Manage., 214 (2018) 184–191.
[45] P. Li, J.E. Zuo, Y.J. Wang, J. Zhao, L. Tang, Z.X. Li, Tertiary nitrogen removal for municipal wastewater using a solid-phase denitrifying biofilter with polycaprolactone as the carbon source and filtration medium, Water Res., 93 (2016) 74–83.
[46] R. Jiang, S. Huang, A.T. Chow, J. Yang, Nitric oxide removal from flue gas with a biotrickling filter using *Pseudomonas putida*, J. Hazard. Mater., 164 (2009) 432–441.
[47] S. Cortez, P. Teixeira, R. Oliveira, M. Mota, Effect of operating parameters on denitrification in an anoxic rotating biological contactor, Environ. Technol., 30 (2009) 1381–1389.